Article

Thermokinetic Study of Catalytic Pyrolysis of Medium-Density Fiberboards over Beta-Zeolite-Supported Platinum

Mateus da Silva Carvalho [1,2], Francieli Martins Mayer [3], Ana Paula Stelzer de Oliveira [3], Doris Ruiz [4], Cesário Francisco das Virgens [5] and Maria do Carmo Rangel [1,3,*]

[1] Escola Politécnica de Engenharia, Universidade Federal da Bahia, Salvador 40210-630, BA, Brazil; carvalho.mateus@ufba.br

[2] Departamento de Ciências Exatas e da Natureza, Universidade Estadual do Sudoeste da Bahia, Itapetinga 45700-000, BA, Brazil

[3] Institute of Chemistry, Universidade Federal do Rio Grande do Sul, Porto Alegre 90650-001, RS, Brazil; francimayer@gmail.com (F.M.M.); anapaulasoliv@gmail.com (A.P.S.d.O.)

[4] Facultad de Ciencias Químicas, Universidad de Concepción, Casilla 160-C, Concepción 4070371, Chile; doruiz@udec.cl

[5] Departamento de Ciências Exatas e da Terra, Universidade do Estado da Bahia, Salvador 41150-000, BA, Brazil; cvirgens@uneb.br

* Correspondence: maria.rangel@ufrgs.br

Abstract: Catalytic pyrolysis is an attractive alternative for converting biomass into energy and chemicals, replacing fossil sources. Efficient catalysts can be used to remove compounds containing oxygen during pyrolysis, improving the bio-oil properties and thus being an important route towards sustainability. Catalytic pyrolysis of medium-density fiberboard (MDF) residues over platinum (1%) supported on beta zeolite was carried out using a biomass/catalyst ratio of 1.0/0.2. The catalysts were characterized via Fourier transform infrared spectroscopy, flame atomic absorption spectrometry, X-ray diffraction, nuclear magnetic resonance, temperature-programmed reduction, and temperature-programmed desorption of ammonia. The thermokinetic and thermodynamic parameters were determined using the isoconversional and non-isothermal methods of Friedman, Flynn-Wall-Ozawa (FWO), and Kissinger-Ahakira-Sunose (KAS). The Friedman method was the most adequate to describe the reaction and thermodynamic parameters. The results show that the catalysts promote the reduction in activation energy compared to non-catalytic pyrolysis. Non-impregnated and impregnated catalysts showed different activation energies and thus different reactions. The addition of platinum slightly increased the activation energy due to the promotion of reactions that require more energy, for example, cracking and coke deposition.

Keywords: beta zeolite; pyrolysis; medium-density fiberboard; thermokinetic conversion; platinum

1. Introduction

Concerns about the growing demand for clean energy have pushed research towards searching for ways to decrease the impact of anthropic activity on the environment. Several initiatives have tried to replace petroleum, for instance, aiming to reduce the emissions of polluting gases into the atmosphere and contributing to mitigating global warming [1–4]. Biomass has been considered as a potential candidate to replace petroleum in the production of green fuels and chemicals, with the advantages of a low price and high availability across the world.

Biomass can be conveniently converted to chemicals and biofuels via catalytic pyrolysis, an efficient and versatile process which allows the tailoring of products for different applications [5]. Zeolites are by far the most studied catalysts for pyrolysis, showing high activity and selectivity thanks to their high acidity, adsorption capacity, and hydrothermal stability, as well as shape selectivity [6,7]. Beta zeolite, for instance, showed high selectivity

to high-value industrial chemicals such as benzene, toluene, ethylbenzene, and xylene (BTEX). In addition, the introduction of nickel largely improved its selectivity to desirable products, decreasing or avoiding toxic polyaromatics [8,9]. Other metals have also shown beneficial behaviors, due to having metallic and acidic sites, which act cooperatively to catalyze different types of reactions. Mayer et al. 2018 [10], for instance, investigated the activity of HZSM-5-supported metals (iron, nickel, cobalt, niobium, and zinc) in the catalytic pyrolysis of MDF residue, and observed high selectivity for the production of BTX when nickel and iron were impregnated on the HZSM-5. The contents of polyaromatics and oxygenates were also reduced when compared to the results achieved when using pure zeolite. Kumar et al. 2020 [11] evaluated the effect of mono- (CuZ and NiZ) and bimetallic (CuNiZ) zeolite catalysts on upgrading bio-oil from the ex situ pyrolysis of pine wood biomass. The authors observed that the mono- and bimetallic catalysts were efficient in the deoxygenation and production of hydrocarbon in comparison with the pure zeolite. The nickel catalyst was more efficient in producing aromatic hydrocarbons and decreasing oxygenates, while copper increased the production of aliphatic hydrocarbons. In general, the bimetallic catalyst produced the highest quality bio-oil. Chen et al. 2019 [12] impregnated 2 wt% zinc, iron, calcium, cerium, or lanthanum on HZSM-5 and investigated the role of these catalysts in the production of BTX through the analytical pyrolysis of sawdust. The study pointed out that zinc and iron were more effective in upgrading biomass pyrolysis vapors, as they promoted the BTX content and reduced oxygenates. All impregnated catalysts reduced naphthalene and methylnaphthalene. The zinc contents in HZSM-5 were also varied, and values between 0.5 and 4 wt% were considered ideal for BTX production.

The thermokinetic study of catalytic pyrolysis provides a powerful tool for investigating the kinetic and thermodynamic parameters required to support the reaction mechanism, using several biomasses over different catalysts. Carvalho et al. 2022 [9], for instance, used the Friedman model to determine the thermokinetic parameters of MDF pyrolysis over beta-zeolite-supported nickel. On the other hand, Camelo et al. 2022 [13] carried out a thermokinetic study of the pyrolysis of *Abelmoschus esculentus* L. Moench over zirconium oxide, observing the occurrence of dehydration reactions and oxidative degradation of the chelating agents present in the biomass. Santos et al. 2022 [14] proposed a new model to determine the degradation kinetics of sisal residue, where a fit model is used to define the reaction order and an isoconversion model is used to obtain the activation energy and pre-exponential factor. The authors conclude that the Friedman model was the only one that presented satisfactory results and had good agreement with the results already reported in the literature using only the free model.

In spite of the large number of papers addressing catalytic pyrolysis, there is still a need to search for new catalysts which allow for the control of the network of reactions that take place during the process. In fact, the mechanisms of biomass pyrolysis are still under investigation, due to the complexity of the lignocellulosic matrix, which generates the simultaneous occurrence of numerous reactions. In addition, both the metal and the support strongly affect the reaction mechanism, determining the products [6–10,12,15]. Therefore, the results obtained over a catalyst cannot be extrapolated to another one. This work aims to determine the thermokinetic and thermodynamic parameters for the pyrolysis of medium-density fiberboard (MDF) residue over beta-zeolite-supported platinum. Thermokinetic parameters were determined using the non-isothermal Friedman, Flynn-Wall-Ozawa (FWO) and Kissinger-Ahakira-Sunose (KAS) models. To our knowledge, this catalyst has never been studied in MDF pyrolysis; this investigation is thus valuable since the catalyst has potential to control the reactions during pyrolysis.

2. Materials and Methods

2.1. Catalyst Preparation

Beta zeolite with a silica-to-alumina ratio (SAR) equal to 30 was synthesized as described elsewhere [8,9], using silica extracted from coal ash from a thermal power plant. The

gel composition obtained was 1.5 Na$_2$O/1 Al$_2$O$_3$/30 SiO$_2$/8.4 TEAOH/315 H$_2$O, where TEAOH is tetraethylammonium hydroxide. The acid form of the catalyst was obtained after being ion-exchanged with ammonium nitrate at 80 °C for 3 h. Beta zeolite was then impregnated with 1 wt% platinum by dispersing the solid in a hexachloroplatinic acid solution and keeping it under agitation for 1 h. The solid was dried at 120 °C for 12 h and heated (2 °C min^{-1}) under air flow up to 550 °C and maintained for 5 h. The catalysts were named B and BP for non-impregnated beta zeolite and beta zeolite impregnated with platinum, respectively.

2.2. Catalyst Characterization

Powder X-ray diffraction (XRD) patterns were recorded on an Ultima IV diffractometer (Rigaku, Honshu, Japan), with Cu-Kα radiation generated at 40 kV and 17 mA, using a monochromator, and in the 2θ range of 5° to 50°. Fourier transform infrared spectroscopy (FT-IR) was carried out on an IR Prestige-21 (Shimadzu, Kyoto, Japan), with a spectral scanning range of 4000 cm^{-1} to 400 cm^{-1}. The silica-to-alumina ratio (SAR) was determined via flame atomic absorption spectrometry (FAAS) using a Perkin-Elmer A Analyst 200 apparatus equipped with a hollow-cathode lamp (LUMINATM, Perkin-Elmer, Waltham, MA, USA).

Nuclear magnetic resonance (NMR) was performed using an 11.7T 500 MHz field device, model dd2 narrowbore from Agilent Technologies. ^{29}Si spectra were obtained with a contact time of 7 ms, relaxation time of 5 s, pw90H1 of 2.9 us, pq90C13 of 2.55 us, and rotor spinning at 10 kHz. ^{27}Al spectra were obtained with a relaxation time of 10 s, pw90Al27 of 14 us, and rotor spinning at 10 kHz. The acidity measurements of catalysts were performed through ammonia temperature-programmed desorption (NH$_3$-TPD) using a Micromeritics AutoChem II equipped with a thermal conductivity detector (TCD). First, the samples were submitted to a pretreatment under helium flow (50 mL min^{-1}) at 110 °C for 60 min. The main experimental conditions were a valve temperature of 110 °C, detector temperature of 100 °C, and filament temperature of 175 °C. The same conditions and equipment were used in the temperature-programmed reduction of hydrogen (H$_2$-TPR) experiments.

2.3. Thermogravimetric Analysis

The biomass used in the pyrolysis experiments was the MDF residue, and M will be used to refer to MDF. The method used for the pretreatment and to determine the chemical composition of MDF were described in previous work [8]. The MDF pyrolysis was carried out on TGA Q50 equipment (V6.7 Build 203, Universal) using approximately 7.0 mg of sample. The MDF and the catalyst (B or BP) were mixed, keeping an MDF-to-catalyst weight ratio of 1/0.2 to obtain MB (MDF/B) and MBP (MDF/BP) samples. The oven was heated from 25 to 900 °C, at heating rates (β) of 5, 10, 15, and 20 °C min^{-1} under nitrogen flow (60 mL min^{-1}). The data obtained were treated as described in previous work [9].

2.4. Thermokinetic Analysis

The isoconversional methods consider the chemical process as a single-step equation which can be described by the fundamental relationship shown in Equation (1), where $k(T)$ is the rate constant as a function of temperature, $f(\alpha)$ is a function related to the chosen reaction model, and α represents the conversion degree.

$$\frac{d\alpha}{dt} = k(T)f(\alpha) \tag{1}$$

Equation (2) shows the calculation of the conversion degree (α), where m_0 and m_f are the initial and final weight of the sample, respectively, and m_t is the weight at any given time.

$$\alpha = \frac{m_0 - m_t}{m_0 - m_f} \tag{2}$$

The $k(T)$ function which appeared in Equation (1) is described by the Arrhenius equation (Equation (3)), where k is the temperature-dependent constant rate, A is the pre-exponential factor, E_A is the activation energy, R is the gas constant, and T is the temperature of the experiment.

$$k(T) = A exp\left(-\frac{E_A}{RT}\right)$$

(3)

Under non-isothermal conditions, the heating rate can be expressed as a function of time as shown in Equation (4), where dT is an infinitesimal temperature change. Substituting Equations (3) and (4) in Equation (1), one obtains Equation (5). Rearranging this equation, one obtains Equation (6) which is introduced into the function $g(\alpha) = \int_0^\alpha \frac{d\alpha}{f(\alpha)}$, to obtain Equation (7) [16,17].

$$\frac{dT}{dt} = \beta$$

(4)

$$\beta\frac{d\alpha}{dT} = A exp\left(-\frac{E_A}{RT}\right)f(\alpha)$$

(5)

$$\frac{d\alpha}{f(\alpha)} = \frac{A}{\beta} exp\left(-\frac{E_A}{RT}\right)$$

(6)

$$g(\alpha) = \int_0^\alpha \frac{d\alpha}{f(\alpha)} = \int_{T_0}^{T_f} \frac{A}{\beta} exp\left(-\frac{E_A}{RT}\right)$$

(7)

2.4.1. Flynn-Wall-Ozawa (FWO) Model

Equation (8) shows an integral method for non-isothermal data developed by Ozawa and Flynn and Wall [18,19]. By plotting $ln(\beta)$ vs. $1/T$, for each conversion degree (α) at several heating rates (β), the activation energy (E_A) can be calculated from the slope of the line, and the pre-exponential factor (A) can be obtained from the y intercept.

$$ln(\beta) = ln\left(\frac{A E_A}{R g(\alpha)}\right) - 5.331 - 1.052\frac{E_A}{RT}$$

(8)

2.4.2. Kissinger-Ahakira-Sunose (KAS) Model

Based on the Kissinger method, the KAS model [20] allows the calculation of the activation energy and frequency factor as shown in Equation (9). The activation energy (E_A) can be calculated from the slope of the line by plotting $ln\left(\frac{\beta}{T^2}\right)$ vs. $1/T$, for each conversion degree (α) at several heating rates (β).

$$ln\left(\frac{\beta}{T^2}\right) = ln\left(\frac{A R}{E_A g(\alpha)}\right) - \frac{E_A}{RT}$$

(9)

2.4.3. Friedman Model

The Friedman model uses a differential isoconversional technique [14] to determine the activation energy (E_A) and frequency factor (A) of the pyrolysis process. This model can be found by rearranging Equation (7).

$$ln\left(\beta\frac{d\alpha}{dT}\right) = [ln(A) \times ln(f(\alpha))] - \frac{E_A}{RT}$$

(10)

2.4.4. Thermodynamic Parameters

Thermodynamic parameters were obtained from Equations (11)–(13), where Kb, h, and T_m represent the Boltzmann constant (1.381×10^{-23} J K^{-1}), the Planck constant (6.626×10^{-34} J s), and the peak temperature DTG (obtained via derivative thermogravimetry), respectively.

$$\Delta H = E_A - RT$$

(11)

$$\Delta G = E_A + RT_m ln \left(\frac{K_b T_m}{hA} \right) \tag{12}$$

$$\Delta S = \left(\frac{\Delta H - \Delta G}{T_m} \right) \tag{13}$$

3. Results and Discussion

3.1. Catalyst Characterization

The XRD patterns of the catalysts showed typical profiles of beta zeolite, regardless of whether platinum was present, as shown in Figure 1, indicating that the beta zeolite structure was kept after impregnation and calcination [8]. Furthermore, there were no diffraction peaks, suggesting that the platinum crystallites were small enough to be detected via XRD. Non-impregnated beta zeolite and beta-zeolite-supported platinum showed different SAR values (29 and 31, respectively), which are both within the experimental error of the analysis.
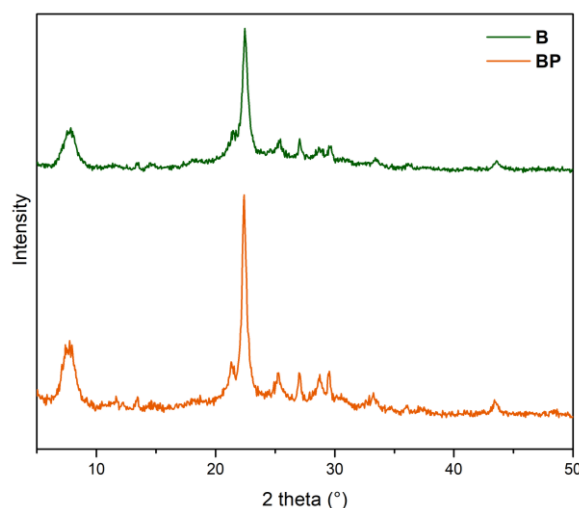

Figure 1. XRD diffractograms for the non-impregnated beta zeolite (B) and beta-zeolite-supported platinum (BP).

Platinum impregnation on beta zeolite decreased the number and the strength of acid sites. After impregnation, the total quantity of acidic sites decreased from 3386 $\mu mol \cdot g^{-1}$ (B) to 2677 $\mu mol \cdot g^{-1}$ (BP). These values are quite different from those obtained for beta zeolite in our previous work [8], probably because of the different source of silica used in each case. In the present work, silica was obtained from coal ashes from a thermal power plant, after treatments were carried out to extract it. The NH$_3$-TPD curve (Figure 2a) shows that the impregnated catalyst had only weak acid sites (T$_{max}$ 196.6 °C), while non-impregnated beta zeolite showed strong (T$_{max}$ 386 °C) and weak acid sites (T$_{max}$ 196 °C). This could be related to the tendency of metals to attach to strong acid sites and then cover them, in accordance with previous work [8,17].

The H$_2$-TPR profile of the impregnated sample presents two platinum reduction peaks (Figure 2b and Table 1). The first peak at a low temperature (166.4 °C) could be attributed to the reduction of PtOx species in a weak interaction with support. The second one at a high temperature (388.1 °C) was assigned to residual platinum oxychlorides (PtOxCly), which are more strongly resistant to reduction and may be incompletely reducible [21,22]. These results show that we can expect that platinum can be easily reduced during pyrolysis by hydrogen provided by cracking reactions.
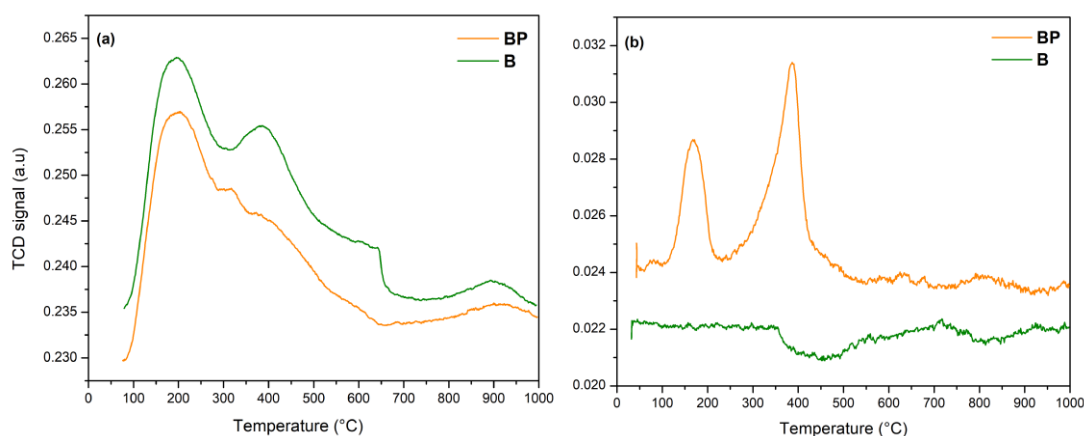
Figure 2. (**a**) NH$_3$-TPD and (**b**) H$_2$-TPR profiles of non-impregnated beta zeolite (B) and (**b**) beta-zeolite-supported platinum (BP).

Table 1. Hydrogen consumption calculated from the TPR curve for beta-zeolite-supported platinum (BP).

Catalyst	Peak Number	Temperature (°C)	Hydrogen Amount (µmol·g^{-1})	Total Hydrogen Amount (µmol·g^{-1})
BP	1	166.4	77.5	237.7
	2	388.1	160.2	

The ^{27}Al NMR spectrum of non-impregnated beta zeolite shows signals centered at 65.7 ppm and 9.1 ppm (Figure 3a). The first is attributed to the tetrahedrally bonded Al atom, while the second is attributed to the octahedrally bonded aluminum atom [8,23]. After platinum impregnation, the spectra showed a small shift of the peak to lower chemical shift values (63.7 ppm), which suggests a shift of aluminum to different crystallographic sites, in agreement with other work [24]. The peaks at 9.1 (B) and 7.9 ppm (BP) were formed after the zeolite calcination step, being ascribed to octahedral Al species and often associated with Lewis acid sites [25,26]. The chemical shift of this species is dependent on the Si/Al ratio and generally varies between 5 and −5 ppm in zeolites with a low SAR and can return to the tetrahedral position through thermal or chemical treatment, and therefore is associated with the octahedral aluminum in the network. Also, in Figure 3a, a decrease in the intensity of the peaks after platinum impregnation can be observed, which may indicate a decrease in the number of strong acid sites [8]. This finding is in agreement with the results of NH$_3$-TPD, showing that one can expect more cracking over B than in BP, considering only the acid sites. However, platinum is also able to produce coke.

Figure 3b shows the ^{29}Si NMR spectra of beta zeolite with a broad peak ranging from −86 to −121 ppm, centered at −101.5 ppm with a shoulder at −109.8 ppm, which indicates the signal overlap caused by silicon atoms in different chemical environments. The signal at −101.5 ppm is the most intense one and suggests the predominance of the silicon atom at the Si(3Si,1OH) site [27]. The signal at −110 ppm suggests the presence of silicon atoms at the Si(4Si) site and is found in beta zeolites with a high SAR [27,28]. The impregnation of platinum on the beta zeolite did not change the chemical environment of the silicon.

3.2. Thermogravimetry Analysis

Figure 4 shows the TG and DTG curves for the samples. The profiles are typical of lignocellulosic biomass decomposition for both catalytic and non-catalytic pyrolysis. It has been observed that the main events are associated with the volatiles lost and cellulose, hemicellulose, and lignin decomposition [29].
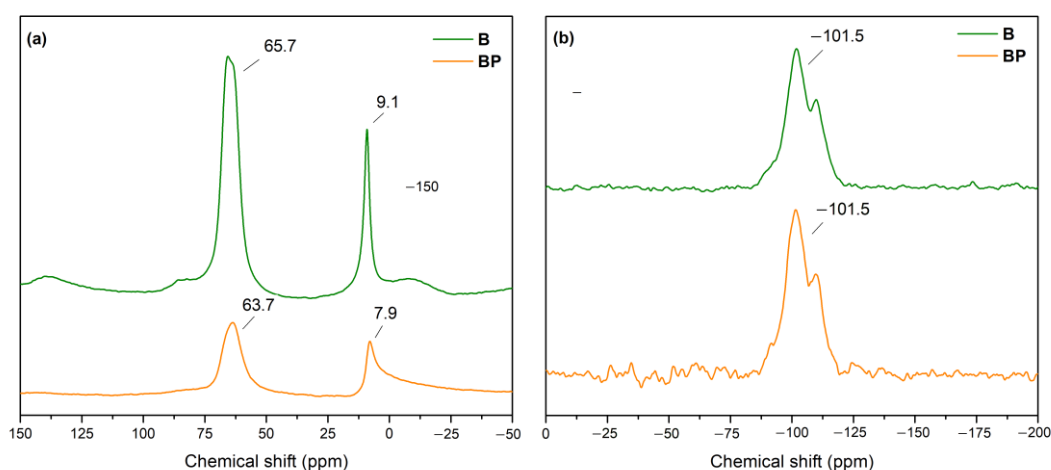
Figure 3. (**a**) ^{27}Al NMR and (**b**) ^{29}Si NMR spectra of non-impregnated beta zeolite (B) and beta-zeolite-supported platinum (BP).
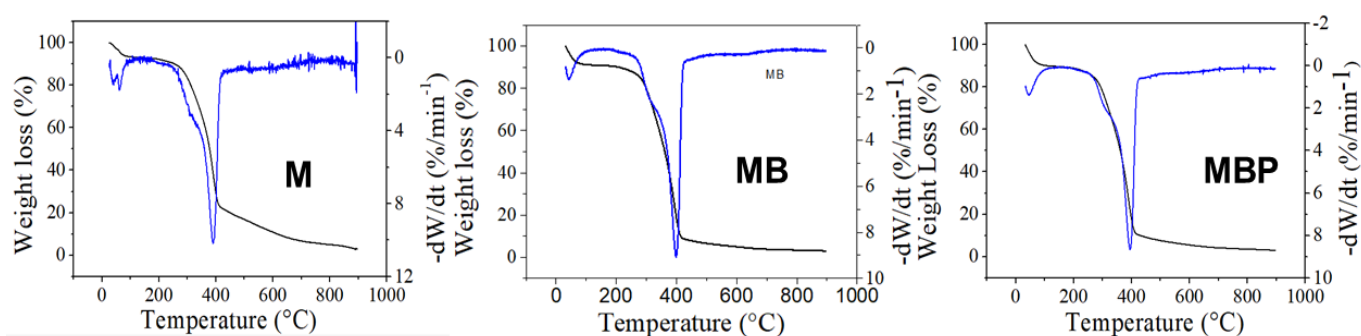

Figure 4. TG (■) and DTG (■) profiles of M (MDF), MB (MDF/non-impregnated beta zeolite), and MBP (MDF/beta-zeolite-supported platinum) samples at the β-heating rate of 10 °C min^{-1}.

The first weight loss (4.58%) started at the beginning of the analysis up to around 114 °C, and is associated with water and nitrogenated compounds from MDF industrial treatment [9,10]. The second stage (200–430 °C) is related to the decomposition of biomass components, comprising a conversion fraction range (α) around ≈10–85% for all samples [9,30], where the decomposition of hemicellulose (200–350 °C), cellulose (300–375 °C), and lignin (250–500 °C) occurs [31,32]. The maximum decomposition, at approximately 390 °C, can be seen in Figure 4. In this temperature range, the system has enough energy to break the C=O, -OH, and C=C bonds of the lignocellulosic matrix to produce liquid and gaseous primary products, such as water, carbon monoxide, and carbon dioxide. Other products are generated in this step, mainly hydrocarbon chains that have a lower molecular weight due to the breakage of side chains and α- and β-aryl-alkyl-ether [9,33,34]. By performing the experiments at different heating rates, the activation energy (E_A) can be calculated. From Figure 5, it can be noted that the maximum rate decomposition decreased with the heating rate. This is because more power heat is supplied to biomass at higher heating rates. In addition, a higher heating rate will take less time to reach equilibrium because of the high heat and mass transfer among the particles. On the other hand, at lower heating rates, the volatiles stay in the reactor for longer, favoring secondary thermal polymerization and condensation reactions. This finding is in accordance with a previous study [15].
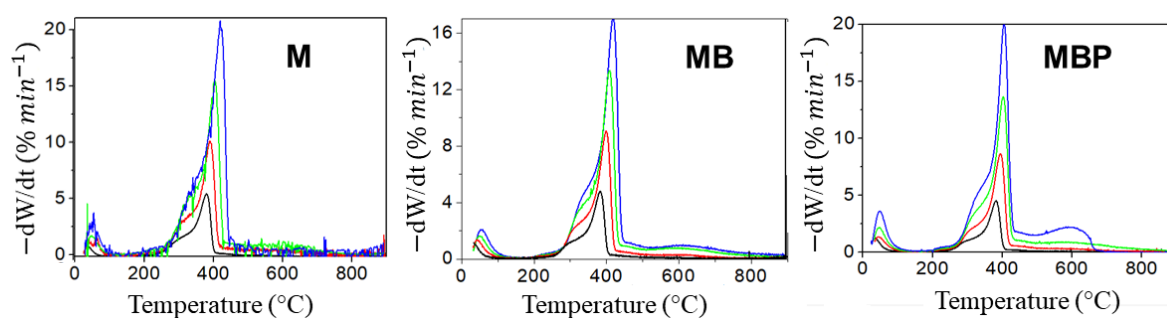
Figure 5. DTG profiles of samples M (MDF), MB (MDF/non-impregnated beta zeolite), and MBP (MDF/beta-zeolite-supported platinum) at β-heating rates of (■) 5 °C min^{-1}; (■) 10 °C min^{-1}; (■) 15 °C min^{-1}; (■) 20 °C min^{-1}.

Table 2 presents the temperature ranges where thermal decomposition events occurred for each sample. We can see that the catalysts accelerated only at Stage III, which is a pseudo-stationary stage due to the slight decomposition occurring until the end of the analysis and is related to other products, such as biochar, which is formed mainly at low heating rates. In this step, some rearrangement reactions occur, such as the production of free radicals and bond breakage [9]. The decomposition of biomass is similar for all samples, discounting the catalyst weight for the catalytic pyrolysis. It can be also noted that similar amounts of coke were produced in all cases.

Table 2. Sample temperature range, percentage biomass decomposition, and residual biochar during non-catalytic pyrolysis and catalytic pyrolysis under a heating rate of β = 10 °C min^{-1}.

Sample	Stage I (°C)	Stage II (°C)	Stage III (°C)	Biomass Decomposition (%)	Biochar (%)
M	25.0–114.0	114.0–413.6	413.6–>900	97.08	2.92
MB	25.0–102.8	102.8–416.3	416.3–763.7	97.06	2.94
MBP	25.0–112.5	112.5–412.4	412.4–791.0	96.98	3.02

The application of the TG data to non-isothermal Friedman, KAS, and FWO methods presented high agreement to experimental data, as indicated by the correlation coefficients (R^2) around 0.9 (Table 3). The correlation index approaches of 1 in all isoconversional methods studied, indicating the other methods can describe the decomposition well, especially at lower conversion fraction values. However, the Friedman model produced the highest correlation factor. Similar results were obtained by Al. Balushi et al. (2023) [35] when evaluating the co-pyrolysis of tire wastes and pine bark. The researchers noted that all the examined methods demonstrated satisfactory fits to the data. Nevertheless, the Friedman method outperformed the others in accurately describing the process and was consequently employed to ascertain the reaction mechanism.

Table 3. Activation energies (E_A/kJ mol^{-1}) for MDF catalytic pyrolysis and non-catalytic pyrolysis calculated using Flynn-Wall-Ozawa (FWO), Kissinger-Akira-Sunose (KAS), and Friedman (F) isoconversional methods. R^2 is the correlation coefficient for each method.

α	Sample M					
	FWO	R^2	KAS	R^2	Friedman	R^2
0.2	120.34	0.9272	116.80	0.9155	116.30	0.9286
0.3	123.58	0.9666	119.78	0.9607	119.39	0.9693
0.4	127.44	0.9865	123.49	0.9841	123.38	0.9894
0.5	128.22	0.9926	124.06	0.9913	124.03	0.9948
0.6	127.90	0.9933	123.56	0.9920	123.82	0.9951
0.7	128.68	0.9968	124.21	0.9961	124.41	0.9980
0.8	100.61	0.8475	94.49	0.8157	94.94	0.9953
Average	122.40	0.9586	118.06	0.9501	118.04	0.9815

Table 3. *Cont.*

α				Sample M		
	FWO	R^2	KAS	R^2	Friedman	R^2
				MB		
0.2	101.32	0.9877	96.71	0.9850	96.43	0.9861
0.3	104.37	0.9887	99.58	0.9865	99.85	0.9877
0.4	109.43	0.9917	104.44	0.9899	104.99	0.9910
0.5	115.55	0.9946	110.63	0.9934	111.37	0.9944
0.6	118.77	0.9954	113.86	0.9944	114.86	0.9955
0.7	118.32	0.9950	113.24	0.9938	114.29	0.9949
0.8	84.39	0.9441	77.29	0.9272	78.48	0.9953
Average	107.45	0.9853	102.25	0.9658	102.90	0.9921
				MBP		
0.2	87.35	0.9400	82.26	0.9264	83.29	0.9384
0.3	107.56	0.9626	102.98	0.9553	104.56	0.9636
0.4	123.16	0.9802	118.99	0.9767	121.04	0.9820
0.5	138.57	0.9875	134.94	0.9855	137.25	0.9884
0.6	147.51	0.9863	144.16	0.9842	146.77	0.9868
0.7	145.48	0.9835	141.88	0.9809	144.56	0.9830
0.8	60.07	0.9867	51.52	0.9847	53.18	0.9876
Average	115.67	0.9753	110.96	0.9705	112.95	0.9757

A small variation in E_A values was observed for different α, indicating good agreement with the isoconversionality principle. As can be seen in Figure 6, the same trend for the E_A and pre-exponential factor was noted for all samples. A reduction in the thermokinetic parameters was observed at $α = 0.8$, indicating the end of the decomposition of the main lignocellulosic components.
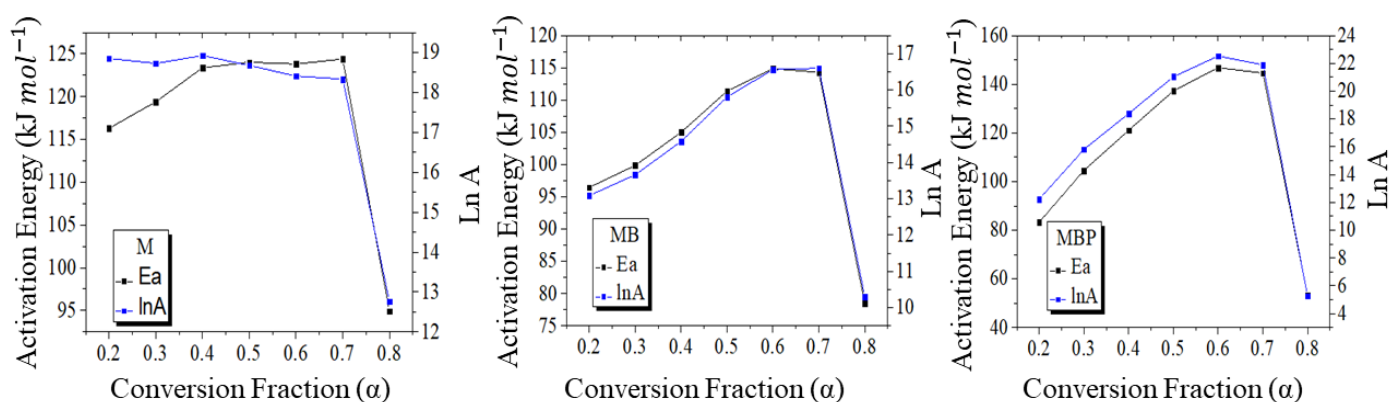

Figure 6. Variation in activation energy (E_A/kJ mol^{-1}) and pre-exponential factor (A) with conversion fraction for M, MB, and MBP samples, calculated using the Friedman model.

The E_A decreased for catalytic pyrolysis compared to the non-catalytic one, for all methods. In addition, as α increased from 0.2 to 0.7, the E_A increased, indicating that the process became more difficult for the reactions involving intermediate compounds. This behavior is related to the decomposition of the main components of the lignocellulosic matrix, such as hemicellulose, cellulose, and lignin, which have long polymeric carbon chains that produce various hydrocarbons and oxygenates of a lower molecular weight. However, a decrease in E_A was observed around 420 °C when α reached values from 0.7 to 0.8, indicating that the process became easier due to the final decomposition of lignin. The average E_A value found for non-catalytic pyrolysis for the Friedman method was 118.04 kJ mol^{-1}, which is higher than that found for the catalytic systems (E_{AMBP} = 112.95 kJ mol^{-1}, E_{AMB} = 102.89 kJ mol^{-1}), indicating that beta zeolite accelerates MDF decomposition. This trend was observed for all conversion fractions (α) evaluated.

However, platinum species on beta zeolite were observed to promote a small increase in the E_A for MBP as compared to MB. This behavior suggests that platinum promotes other

reactions, such as lignin cracking and open-ring reaction aromatization, acting cooperatively with the active sites [36,37] and requiring more energy to occur. The E_A decreased in the following order: $E_{AM} > E_{AMBP} > E_{AMB}$. The thermodynamic results, calculated from data obtained using the Friedman model, are presented in Table 4. The values obtained for Gibbs free energy (ΔG) showed small differences, as observed by Carvalho et al., 2022 [9] when carrying out the pyrolysis of MDF over beta-zeolite-supported nickel. This behavior can be attributed to the different reaction pathways promoted by the catalysts in catalytic pyrolysis.

Table 4. Thermodynamic parameters for catalytic (MB and MBP) and non-catalytic pyrolysis (M).

| α | **M** | | |
	ΔG (kJ mol^{-1})	ΔH (kJ mol^{-1})	ΔS (kJ mol^{-1} K)
0.2	179.25	110.79	−0.10
0.3	181.43	117.80	−0.10
0.4	181.94	119.39	−0.09
0.5	185.28	121.36	−0.10
0.6	188.77	123.38	−0.10
0.7	189.58	123.77	−0.10
0.8	220.58	124.03	−0.15
Average	189.55	120.07	−0.10
α	**MB**		
	ΔG (kJ mol^{-1})	ΔH (kJ mol^{-1})	ΔS (kJ mol^{-1} K)
0.2	90.84	192.42	−0.15
0.3	92.62	191.00	−0.15
0.4	94.27	187.52	−0.14
0.5	96.47	182.87	−0.13
0.6	99.40	181.60	−0.12
0.7	102.73	184.71	−0.12
0.8	105.78	222.90	−0.17
Average	191.86	97.45	−0.14
α	**MBP**		
	ΔG (kJ mol^{-1})	ΔH (kJ mol^{-1})	ΔS (kJ mol^{-1} K)
0.2	184.04	83.29	−0.15
0.3	185.37	104.56	−0.12
0.4	187.41	121.04	−0.10
0.5	188.86	137.25	−0.08
0.6	190.07	146.77	−0.06
0.7	191.36	144.56	−0.07
0.8	192.81	53.18	−0.21
Average	188.59	112.95	−0.11

For the entire range of conversion fractions (α), an increase in ΔG was noted, which was probably due to the lignocellulosic matrix's complexity. The determined value of ΔG for the reaction was positive, indicating that the reaction does not occur spontaneously. It is evident that the thermal degradation process is a non-spontaneous phenomenon, as reflected by the negative entropy (ΔS) and positive ΔG [38,39]. Enthalpy (ΔH) values also changed among the samples, following the order of $\Delta H_{MB} < \Delta H_{MBP} < \Delta H_M$, indicating a less endothermic global process for MB. This result indicates that exothermic reactions are more favorable for non-impregnated beta zeolite. Furthermore, the ΔS values were slightly negative. This phenomenon arises from the transformation of a highly organized structure into a less organized one as the heating rate increases, suggesting that the formation of the activated complex corresponds to a decrease in entropy. This indicates that the activated complex possesses a higher degree of organization compared to the initial substance, as entropy typically measures the level of randomness. The sample likely underwent various chemical or physical aging processes due to thermal effects, ultimately reaching a state of thermodynamic equilibrium [40].

4. Conclusions

The catalytic pyrolysis of biomass using beta zeolite with and without platinum accelerates the decomposition of the third stage of MDF residue decomposition. This indicates that the decrease in the number of strong acid sites after impregnation did not significantly affect the performance of beta-zeolite-supported platinum. Beta zeolite promotes a decrease in activation energy for the MDF pyrolysis process when compared to non-catalytic pyrolysis. However, beta-zeolite-supported platinum presented a slightly higher activation energy compared to non-impregnated beta zeolite. The activation energy follows the order $E_{AMB} < E_{AMBP} < E_{AM}$. This was attributed to the ability of platinum to catalyze other reactions, such as cracking and coke formation. The same trend was observed for enthalpy values, indicating that exothermic reactions are favored by non-impregnated beta zeolite. Gibbs free energy also shows differences between processes. This behavior is attributed to the occurrence of different reactions during the pyrolysis process.

Author Contributions: Conceptualization, methodology, writing—original draft preparation, writing—review and editing: M.d.S.C., A.P.S.d.O. and F.M.M. Methodology: D.R. Conceptualization, writing—original draft preparation, writing—review and editing, supervision: C.F.d.V. and M.d.C.R. All authors have read and agreed to the published version of the manuscript.

Institutional Review Board Statement: Not applicable.

Informed Consent Statement: Not applicable.

Data Availability Statement: Not applicable.

References

1. Zhu, Q.-L.; Wu, B.; Pisutpaisal, N.; Wang, Y.-W.; Ma, K.-D.; Dai, L.-C.; Qin, H.; Tan, F.-R.; Maeda, T.; Xu, Y.-S.; et al. Bioenergy from dairy manure: Technologies, challenges and opportunities. *Sci. Total Environ.* **2021**, *790*, 148199. [CrossRef] [PubMed]
2. Okolie, J.A.; Mukherjee, A.; Nanda, S.; Dalai, A.K.; Kozinski, J.A. Next-generation biofuels and platform biochemicals from lignocellulosic biomass. *Int. J. Energy Res.* **2021**, *45*, 14145–14169. [CrossRef]
3. Dey, S.; Reang, N.; Das, P.; Deb, M. A comprehensive study on prospects of economy, environment, and efficiency of palm oil biodiesel as a renewable fuel. *J. Clean. Prod.* **2020**, *286*, 124981. [CrossRef]
4. Si, Z.; Zhang, X.; Wang, C.; Ma, L.; Dong, R. An Overview on Catalytic Hydrodeoxygenation of Pyrolysis Oil and Its Model Compounds. *Catalysts* **2017**, *7*, 169. [CrossRef]
5. Seo, M.W.; Lee, S.H.; Nam, H.; Lee, D.; Tokmurzin, D.; Wang, S.; Park, Y.-K. Recent advances of thermochemical conversion processes for biorefinery. *Bioresour. Technol.* **2021**, *343*, 126109. [CrossRef]
6. Rangel, M.D.C.; Mayer, F.M.; Carvalho, M.D.S.; Saboia, G.; de Andrade, A.M. Selecting Catalysts for Pyrolysis of Lignocellulosic Biomass. *Biomass* **2023**, *3*, 31–63. [CrossRef]
7. Rangel, M.C.; Carvalho, M.D.S.; Mayer, F.M.; Saboia, G.; de Andrade, A.M.; de Oliveira, A.P.S.; Santos, P.L.D. Improving Fast Pyrolysis by Tailoring High-Quality Products Using Catalysts. In *Advances in Chemistry Research*, 1st ed.; Taylor, J., Ed.; Nova Publishers: New York, NY, USA, 2022; Volume 75, pp. 119–169.
8. Mayer, F.M.; de Oliveira, A.P.S.; Junior, D.L.d.O.; Agustini, B.C.; da Silva, G.A.; Tanabe, E.H.; Ruiz, D.; Rangel, M.D.C.; Zini, C.A. Influence of Nickel Modified Beta Zeolite in the Production of BTEX During Analytical Pyrolysis of Medium-Density Fiberboard (MDF). *Waste Biomass Valoriz.* **2021**, *13*, 1717–1729. [CrossRef]
9. Carvalho, M.; Oliveira, A.P.; Mayer, F.; Virgens, C.; Rangel, M.D.C. Thermokinetic and Thermodynamic Parameters for Catalytic Pyrolysis of Medium Density Fiber over Ni/Beta Zeolite. *Catal. Res.* **2022**, *2*, 38. [CrossRef]
10. Mayer, F.M.; Teixeira, C.M.; Pacheco, J.G.A.; de Souza, C.T.; Bauer, D.d.V.; Caramão, E.B.; Espíndola, J.d.S.; Trierweiler, J.O.; Lopez, O.W.P.; Zini, C.A. Characterization of analytical fast pyrolysis vapors of medium-density fiberboard (mdf) using metal-modified HZSM-5. *J. Anal. Appl. Pyrolysis* **2018**, *136*, 87–95. [CrossRef]
11. Kumar, R.; Strezov, V.; Kan, T.; Weldekidan, H.; He, J.; Jahan, S. Investigating the Effect of Mono- and Bimetallic/Zeolite Catalysts on Hydrocarbon Production during Bio-oil Upgrading from *Ex Situ* Pyrolysis of Biomass. *Energy Fuels* **2019**, *34*, 389–400. [CrossRef]
12. Che, Q.; Yang, M.; Wang, X.; Yang, Q.; Williams, L.R.; Yang, H.; Zou, J.; Zeng, K.; Zhu, Y.; Chen, Y.; et al. Influence of physicochemical properties of metal modified ZSM-5 catalyst on benzene, toluene and xylene production from biomass catalytic pyrolysis. *Bioresour. Technol.* **2019**, *278*, 248–254. [CrossRef] [PubMed]
13. Camelo, E.R.; Castro, J.D.S.; das Virgens, C.F. Thermokinetic evaluation of zircon oxide green synthesis mediated by plant extract of *Abelmoschus esculentus* L. Moench. *J. Therm. Anal. Calorim.* **2022**, *148*, 49–62. [CrossRef]

14. Santos, D.B.P.; de Jesus, M.F.; Júnior, J.M.F.; Pires, C.A.D.M. Determination of kinetic parameters for the sisal residue pyrolysis through thermal analysis. *J. Ind. Eng. Chem.* **2022**, *109*, 296–305. [CrossRef]

15. Loy, A.C.M.; Yusup, S.; Lam, M.K.; Chin, B.L.F.; Shahbaz, M.; Yamamoto, A.; Acda, M.N. The effect of industrial waste coal bottom ash as catalyst in catalytic pyrolysis of rice husk for syngas production. *Energy Convers. Manag.* **2018**, *165*, 541–554. [CrossRef]

16. Brown, M.E. (Ed.) *Introduction to Thermal Analysis: Techniques and Applications*; Springer: Dordrecht, The Netherlands, 2001.

17. Vyazovkin, S.; Burnham, A.K.; Criado, J.M.; Pérez-Maqueda, L.A.; Popescu, C.; Sbirrazzuoli, N. ICTAC Kinetics Committee recommendations for performing kinetic computations on thermal analysis data. *Thermochim. Acta* **2011**, *520*, 1–19. [CrossRef]

18. Ozawa, T. A New Method of Analyzing Thermogravimetric Data. *Bull. Chem. Soc. Jpn.* **1965**, *38*, 1881–1886. [CrossRef]

19. Flynn, J.H.; Wall, L.A. General treatment of the thermogravimetry of polymers. *J. Res. Natl. Bur. Stand. Sect. A Phys. Chem.* **1966**, *70A*, 487–523. [CrossRef]

20. Kissinger, H.E. Variation of peak temperature with heating rate in differential thermal analysis. *J. Res. Natl. Bur. Stand.* **1956**, *57*, 217. [CrossRef]

21. Loiha, S.; Föttinger, K.; Zorn, K.; Klysubun, W.; Rupprechter, G.; Wittayakun, J. Catalytic enhancement of platinum supported on zeolite beta for toluene hydrogenation by addition of palladium. *J. Ind. Eng. Chem.* **2009**, *15*, 819–823. [CrossRef]

22. Aboul-Gheit, A.K.; Aboul-Fotouh, S.M. Insight in cyclohexene hydroconversion process using catalysts containing 0.35% Pt on amorphous and zeolite supports. *J. Taiwan Inst. Chem. Eng.* **2012**, *43*, 711–717. [CrossRef]

23. Grecco, S.; Gomes, L.; Reyes, P.; Oportus, M.; Rangel, M. Effect of platinum on the activity of zeolite-based catalysts. *Stud. Surf. Sci. Catal.* **2005**, *158*, 1937–1944. [CrossRef]

24. Dirken, P.J.; Kentgens, A.P.M.; Nachtegaal, G.H.; van der Eerden, A.M.J.; Jansen, J.B.H. Solid-state MAS NMR study of pentameric aluminosilicate groups with 180 degrees intertetrahedral Al-O-Si angles in zunyite and harkerite. *Am. Miner.* **1995**, *80*, 39–45. [CrossRef]

25. Teh, L.; Setiabudi, H.; Sidik, S.; Annuar, N.; Jalil, A. Synergic role of platinum (Pt) and molybdenum trioxide (MoO_3) promoted HBEA zeolite towards n-heptane isomerization. *Mater. Chem. Phys.* **2021**, *263*, 124406. [CrossRef]

26. Kunkeler, P.; Zuurdeeg, B.; van der Waal, J.; van Bokhoven, J.; Koningsberger, D.; van Bekkum, H. Zeolite Beta: The Relationship between Calcination Procedure, Aluminum Configuration, and Lewis Acidity. *J. Catal.* **1998**, *180*, 234–244. [CrossRef]

27. Abraham, A.; Lee, S.-H.; Shin, C.-H.; Hong, S.B.; Prins, R.; van Bokhoven, J.A. Influence of framework silicon to aluminium ratio on aluminium coordination and distribution in zeolite Beta investigated by 27Al MAS and 27Al MQ MAS NMR. *Phys. Chem. Chem. Phys.* **2004**, *6*, 3031–3036. [CrossRef]

28. Pérez-Pariente, J.; Sanz, J.; Fornés, V.; Corma, A. ^{29}Si and ^{27}Al MAS NMR Study of Zeolite with Different Si/Al Ratios. *J. Phys. Chem.* **1990**, *124*, 217–223. [CrossRef]

29. Stelzer, J.; Paulus, M.; Hunger, M.; Weitkamp, J. Hydrophobic properties of all-silica zeolite beta. *Microporous Mesoporous Mater.* **1998**, *22*, 1–8. [CrossRef]

30. Castro, J.D.S.; da Silva, E.G.P.; Virgens, C.F. Evaluation of models to predict the influence of chemical pretreatment on the peels of *Nephelium lappaceum* L. based on pyrolysis kinetic parameters obtained using a combined Fraser-Suzuki function and Friedman's isoconversional method. *J. Anal. Appl. Pyrolysis* **2020**, *149*, 104827. [CrossRef]

31. Jaffar, M.M.; Nahil, M.A.; Williams, P.T. Pyrolysis-catalytic hydrogenation of cellulose-hemicellulose-lignin and biomass agricultural wastes for synthetic natural gas production. *J. Anal. Appl. Pyrolysis* **2019**, *145*, 104753. [CrossRef]

32. Iqbal, A.; Noreen, N.; Imran, M.; Alves, J.L.F.; da Silva, J.C.G.; Badshah, S.L. Valorization of the biomass of *Rhizoclonium hookeri* through slow pyrolysis and its thermokinetic investigation for bioenergy potential. *Biomass Bioenergy* **2023**, *168*, 106690. [CrossRef]

33. Carvalho, M.D.S.; das Virgens, C.F.; Carneiro, L.L.; da Silva, E.G.P.; das Chagas, T.P. Prediction of alkaline treatment effect on the slow pyrolysis of the *Pachira aquatica* Aubl. Fruit bark using artificial neural networks. *Braz. J. Dev.* **2020**, *6*, 80216–80235. [CrossRef]

34. Aslan, D.I.; Özoğul, B.; Ceylan, S.; Geyikçi, F. Thermokinetic analysis and product characterization of Medium Density Fiberboard pyrolysis. *Bioresour. Technol.* **2018**, *258*, 105–110. [CrossRef] [PubMed]

35. Al-Balushi, F.A.; Burra, K.G.; Chai, Y.; Wang, M. Co-pyrolysis of waste tyre and pine bark: Study of reaction kinetics and mechanisms. *Biomass Bioenergy* **2023**, *168*, 106654. [CrossRef]

36. Plata, D.B.; Infantes-Molina, A.; Rodríguez-Castellón, E. Study of bifunctionality of Pt/SBA-15 catalysts for HDO of Dibenzofuran reaction: Addition of Mo or use of an acidic support. *Appl. Catal. A Gen.* **2019**, *580*, 93–101. [CrossRef]

37. Zheng, Y.; Wang, J.; Li, D.; Liu, C.; Lu, Y.; Lin, X.; Zheng, Z. Highly efficient catalytic pyrolysis of biomass vapors upgraded into jet fuel range hydrocarbon-rich bio-oil over a bimetallic Pt–Ni/γ-Al_2O_3 catalyst. *Int. J. Hydrogen Energy* **2021**, *46*, 27922–27940. [CrossRef]

38. Pattanayak, S.; Hauchhum, L.; Loha, C.; Sailo, L.; Mishra, L. Experimental investigation on pyrolysis kinetics, reaction mechanisms and thermodynamic parameters of biomass and tar in N_2 atmosphere. *Sustain. Energy Technol. Assess.* **2021**, *48*, 101632. [CrossRef]

39. Bieniek, A.; Reinmöller, M.; Küster, F.; Gräbner, M.; Jerzak, W.; Magdziarz, A. Investigation and modelling of the pyrolysis kinetics of industrial biomass wastes. *J. Environ. Manag.* **2022**, *319*, 115707. [CrossRef]

40. Gouda, N.; Panda, A.K. Determination of kinetic and thermodynamic parameters of thermal degradation of different biomasses for pyrolysis. *Biocatal. Agric. Biotechnol.* **2019**, *21*, 101315. [CrossRef]